The Astrophysical Journal, 736:77 (8pp), 2011 August 1 doi:10.1088/0004-637X/736/2/77

AN Hα NUCLEAR SPIRAL STRUCTURE IN THE E0 ACTIVE GALAXY Arp 102B

Kambiz Fathi[1,2,3,9], David J. Axon[3,4], Thaisa Storchi-Bergmann[5], Preeti Kharb[3], Andrew Robinson[3], Alessandro Marconi[6], Witold Maciejewski[7], and Alessandro Capetti[8]
[1] Instituto de Astrofísica de Canarias, 38200 La Laguna, Spain; fathi@iac.es
[2] Department of Astronomy, Stockholm University, AlbaNova, SE-106 91 Stockholm, Sweden
[3] Department of Physics, Rochester Institute of Technology, 85 Lomb Memorial Drive, Rochester, NY 14623, USA; djasps@rit.edu, axrsps@rit.edu, pxksps@cis.rit.edu
[4] School of Mathematical and Physical Sciences, University of Sussex, Brighton BN1 9QH, UK
[5] Instituto de Fisica, UFRGS, Av. Bento Goncalves 9500, 91501-970 Porto Alegre RS, Brazil; thaisa@ufrgs.br
[6] INAF-Osservatorio Astrofisico di Arcetri, Largo Fermi 5, I-50125 Firenze, Italy; marconi@arcetri.astro.it
[7] Astrophysics Research Institute, Liverpool John Moores University, Twelve Quays House, Egerton Wharf, Birkenhead, CH41 1LD, UK; wxm@astro.livjm.ac.uk
[8] INAF-Osservatorio Astronomico di Torino, Strada Osservatorio 20, 10025 Pino Torinese, Italy; capetti@to.astro.it
Received 2010 December 16; accepted 2011 May 1; published 2011 July 7

ABSTRACT

We report the discovery of a two-armed mini-spiral structure within the inner kiloparsec of the E0 LINER/Seyfert 1 galaxy Arp 102B. The arms are observed in Hα emission and located east and west of the nucleus, extending up to ≈1 kpc from it. We use narrow-band imaging from the *Hubble Space Telescope* Advanced Camera for Surveys, in combination with archival Very Large Array radio images at 3.6 and 6 cm to investigate the origin of the nuclear spiral. From the Hα luminosity of the spiral, we obtain an ionized gas mass of the order of 10^6 solar masses. One possibility is that the nuclear spiral represents a gas inflow triggered by a recent accretion event which has replenished the accretion disk, giving rise to the double-peaked emission-line profiles characteristic of Arp 102B. However, the radio images show a one-sided curved jet which correlates with the eastern spiral arm observed in the Hα image. A published milliarcsecond radio image also shows a one-sided structure at position angle ≈40°, approximately aligned with the inner part of the eastern spiral arm. The absence of a radio counterpart to the western spiral arm is tentatively interpreted as indicating that the jet is relativistic, with an estimated speed of 0.45*c*. Estimates of the jet kinetic energy and the ionizing luminosity of the active nucleus indicate that both are capable of ionizing the gas along the spiral arms. We conclude that, although the gas in the nuclear region may have originated in an accretion event, the mini spiral is most likely the result of a jet–cloud interaction rather than an inflowing stream.

Key words: galaxies: active – galaxies: individual (Arp 102B) – galaxies: kinematics and dynamics – galaxies: nuclei

Online-only material: color figure

1. INTRODUCTION

Over the past few years, observations of the central regions of active galaxies have shown that nuclear structures (within the inner kpc), such as bars, rings, and spirals, seem to be ubiquitous (e.g., Pogge & Martini 2002; Fathi 2004; Jogee et al. 2005). The most common nuclear structures are dusty spirals which are estimated to reside in more than half of all active galaxies. The enhanced frequency of nuclear spirals in active galaxies as compared to non-active galaxies (e.g., Martini et al. 2003), and in particular in early-type hosts (Simões Lopes et al. 2007), supports the hypothesis that nuclear spirals are a mechanism for fueling the nuclear supermassive black hole (hereafter SMBH). This has now been confirmed by a few studies such as in the LINER/Seyfert 1 galaxy NGC 1097 (Fathi et al. 2006; Davies et al. 2009; van de Ven & Fathi 2010), in the LINER galaxy NGC 6951 (Storchi-Bergmann et al. 2007), NGC 4051 (Riffel et al. 2008), NGC 1068 (Müller Sánchez et al. 2009), and M81 (Schnorr Müller et al. 2011), using two-dimensional spectroscopy together with high-resolution imaging to map the nuclear spiral arms. These authors have measured the gas emission-line kinematics in the spiral arms, confirming gas streaming from scales of hundred of parsecs toward the nucleus.

Morphologically, nuclear spirals are divided into two main categories, chaotic spirals and symmetric or grand-design spirals, for which different formation mechanisms have been proposed. Chaotic spiral arms could be formed by acoustic instability (Elmegreen et al. 1998; Montenegro et al. 1999), whereas grand-design spirals could form by density waves (Englmaier & Shlosman 2000; Saijo et al. 2003) or by hydrodynamic shocks induced by non-axisymmetric potentials (Maciejewski et al. 2002). Martini & Pogge (1999) have shown that nuclear spirals are not self-gravitating, and that they are likely to be shocks in the nuclear gas disks (e.g., Yuan & Yen 2004). Maciejewski (2004a, 2004b) has demonstrated that, if a central SMBH is present, spiral shocks can extend all the way to its vicinity and generate gas inflow compatible to the accretion rates observed in local active galactic nuclei (AGNs).

The nuclear spirals are distinct from the spiral arms in the disks of galaxies as they seem to have lower density contrasts and no associated star formation. Possible ionization mechanisms for the emission-line gas observed (e.g., in NGC 1097; Storchi-Bergmann et al. 1996; Fathi et al. 2006, or NGC 2974; Emsellem et al. 2003) are the spiral shocks, normally with velocities of the order of ≈100 km s^{-1} and photoionization by an active nucleus.

Here we report the discovery of a nuclear spiral in the inner kiloparsec of the LINER/Seyfert 1 galaxy Arp 102B. Although

[9] A major part of this work was completed at RIT.

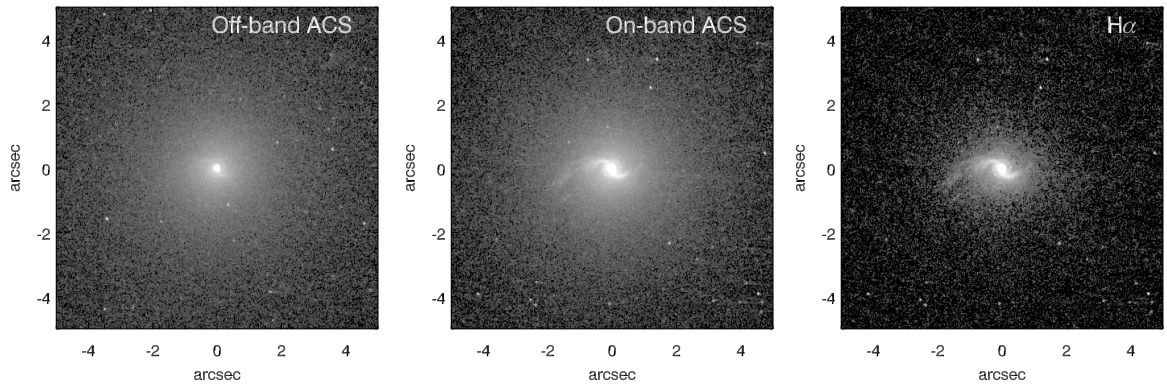

Figure 1. From left to right: our *"off-band" HST*-ACS continuum image, *"on-band" HST*-ACS ramp filter image, and continuum-subtracted Hα emission-line image. In all panels, north is up and east is to the left.

mini spirals have been observed in other galaxies, as pointed out above, the case of Arp 102B is particularly interesting because the host galaxy is a "featureless" E0 galaxy. Another peculiar characteristic of Arp 102B is the presence of very broad ($\approx$15,000 km s^{-1}) double-peaked emission lines in its nuclear spectrum, similar to what is observed in NGC 1097 (Storchi-Bergmann et al. 1993, 2003; Fathi et al. 2006) and also in some other LINERs, e.g., M81 (Bower et al. 1996), NGC 4203 (Shields et al. 2000), NGC 4450 (Ho et al. 2000), and NGC 4579 (Barth et al. 2001), as well as in radio galaxies (e.g., Eracleous & Halpern 1994; Lewis et al. 2010). In fact, Arp 102B is considered to be the prototypical "double-peaker" (Chen et al. 1989; Newman et al. 1997; Gezari et al. 2007; Flohic & Eracleous 2008).

We speculate that the appearance of double-peaked lines is related to a recent accretion event. This seems to be the case for NGC 1097, M81, and for some of the other LINERs above, which had not shown double-peaked lines in previous observations. It thus may be that the nuclear spiral in Arp 102B is also a tracer of this accretion event. As noted above, nuclear spirals are also present in NGC 1097, M81, and other LINERs with double-peaked lines.

In this work, we present high-resolution *Hubble Space Telescope* images acquired with the Advanced Camera for Surveys (*HST*-ACS) in both the narrow-band Hα and the continuum. These data are described in Sections 2 and 3. In Section 4, we present unpublished archival Very Large Array (VLA) radio images; in Section 5, we compare the *HST* and VLA data discussing the relationship between the radio structure and the spiral arms of the galaxy; and in Section 6, we present our conclusions.

2. *HST* OBSERVATIONS

HST data (GO 9782; PI: David J. Axon) were obtained as part of a larger program to study circumnuclear gas kinematics in objects with double-peaked broad lines. *HST*-ACS images of Arp 102B were obtained using the high-resolution camera (0.″025 pixel^{-1} and a field of view of 26″ × 29″) through the FR656N filter (for the continuum) and the 6722 Å linear ramp filter centered on the H$\alpha\lambda$6563 emission line at the redshift ($z = 0.0242$) of Arp 102B. The ACS images were reduced and flux calibrated using the standard Calacs pipeline (Pavlovsky et al. 2005). After reduction, the scaled continuum image was subtracted from the linear ramp filter image in order to isolate the pure Hα emission (see Figure 1). In order to remove the point-spread function (PSF) distortion and unveil the underlying structure in the ACS image, we deconvolved the image using

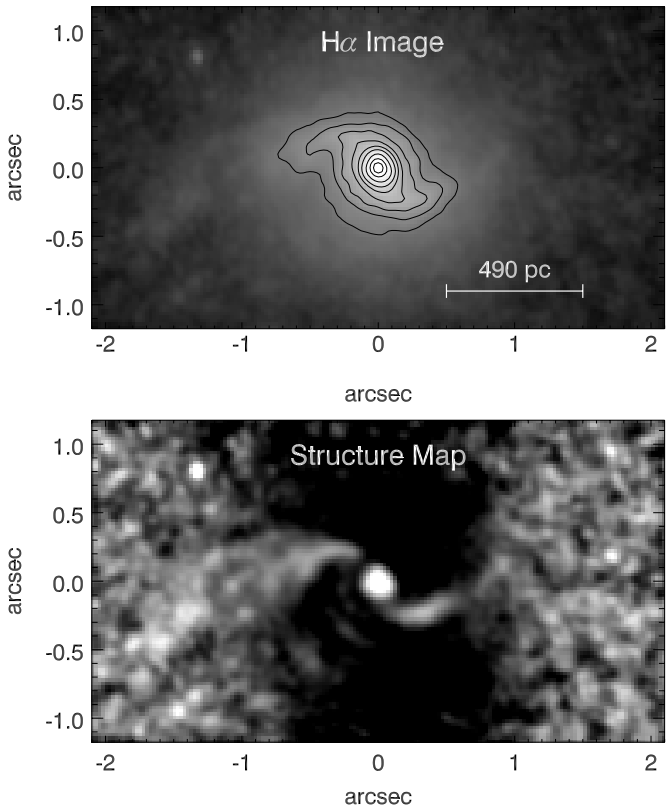

Figure 2. Zooming into the central few hundreds of parsecs of Arp 102B. Top panel: H$\alpha\lambda$6563 image; Bottom panel: the structure map obtained from this image. Both panels have the same orientation as Figure 1.

50–150 Richardson–Lucy iterations (Richardson 1972; Lucy 1974) in conjunction with a PSF model constructed using Tiny Tim (Krist & Hook 1999). Different numbers of iterations produced similar results, and in all cases the final resolution of the image was comparable to that of the original ACS image (i.e., 0.″05), all showing a smooth underlying flux distribution with very prominent nuclear spiral arms in Hα emission.

3. *HST* RESULTS

In the central and right panels of Figure 1, the Hα ramp filter and continuum-subtracted Hα images show two small spiral arms, one to the east and the other to the west of the nucleus. The arm to the west extends to $\approx$1″ while the one to the east extends to $\approx$2″ from the nucleus; in the outer parts, the east arm shows a broader and more "fragmented" structure. In Figure 2,

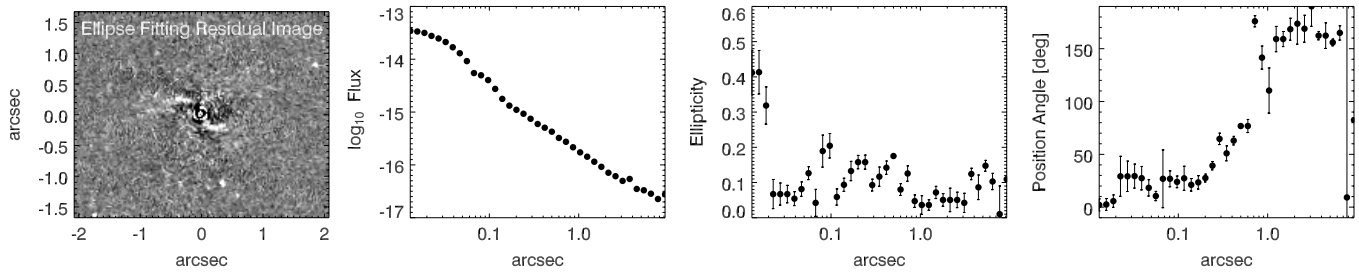

Figure 3. Ellipse fitting results for the continuum image of Arp 102B. In the left panel, we show the residual image obtained from the subtraction of a smooth elliptical model from the continuum image, where the flux is given in erg^{-1} cm^{-2} Å^{-1} arcsec^{-2}. In the panels to the right, we show the radial variation of the parameters of the ellipses.

we show the central $4'' \times 2''$ section of the continuum-subtracted H$\alpha\lambda$6563 image together with a structure map of this image, built in order to increase the contrast and better reveal the spiral morphology.

The structure map technique was proposed by Pogge & Martini (2002) and is based on the Richardson–Lucy image restoration algorithm (Richardson 1972; Lucy 1974) applied to *HST* imaging (e.g., Snyder et al. 1993). The image generated is called the structure map S and is given by

$$S = \left[\frac{I}{I \otimes P}\right] P^t, \quad (1)$$

where I is the original image, P is the model PSF, constructed with the Tiny Tim software (Krist & Hook 1999), P^t is the transpose of the model PSF, and $\otimes$ is the convolution operator. This technique removes the large-scale smooth distribution, highlighting both dust (dark regions) and emission structures (bright regions) with high fidelity. In the structure map, the spiral arms can be traced down to the central 0.″1 (corresponding to ≈50 pc at the galaxy[10]).

In order to investigate the morphology of the continuum image, we fitted an elliptical model (concentric ellipses) to the inner 8″and found a mean ellipticity of 0.098 ± 0.059. The results of this fit are shown in Figure 3. The position of the nucleus—considered to be the center of the elliptical isophotes—did not vary by more than 0.5 pixel. Within the fitted range, the position angle (P.A.) of the ellipses varies by almost 160°, but the ellipticity is small and shows no systematic variations, suggesting that the position angle variation is not significant. The residual between the continuum image and the elliptical model (left panel of Figure 3) shows that the continuum also displays the spiral arms that we have found in the Hα image. This suggests that the continuum image may not be displaying the pure stellar component, including some contribution from nebular emission lines, in particular the [O I]$\lambda\lambda$6300,6364 doublet. An estimate of the contribution of the [O I] emission to the continuum image can be obtained from the [O I]λ6300 line flux from the ground-based optical spectrum of Arp 102B included in the work by Halpern et al. (1996). This spectrum was obtained through an aperture of width 2″ and length 4″, oriented at P.A. = 80°, which approximately matches the size and orientation of the Hα mini spiral, and have emission-line fluxes of 1.9×10^{-14} erg cm^{-2} s^{-1} and 4.3×10^{-14} erg cm^{-2} s^{-1} for [O I]λ6300 and the narrow component of Hα, respectively, thus corresponding to [O I]/Hα = 0.45. Considering that our narrow-band Hα image includes also contribution from the [N II]$\lambda\lambda$6548,84 doublet, an estimate for the ratio between the residual image (continuum–elliptical model), under the assumption that this residual is due to [O I] emission, and the continuum-subtracted Hα image should be of the order of 0.2. This is indeed the approximate value we obtain for the ratio between the two images in the arms, supporting that the residual arms in the continuum are indeed due to contamination by the [O I]λ6300 emission line.

We have integrated the flux in the continuum-subtracted Hα image obtaining 2.31×10^{-13} erg cm^{-2} s^{-1}, but this includes the double-peaked and broad components of the Hα line, which contribute most of the flux in the inner pixels. Performing aperture photometry within a radius of 5 pixels around the nucleus, we estimate that the contribution of the nuclear (broad and double-peaked) components to the total Hα flux is at least 50%. Considering, in addition, that the filter includes also the [N II]$\lambda\lambda$6548,84 emission lines (which together have similar fluxes to that of narrow Hα), we estimate that the total flux in the narrow Hα component is $(5.8 \pm 1.7) \times 10^{-14}$ erg cm^{-2} s^{-1}. Within the uncertainties, this value is consistent with the one reported by Halpern et al. (1996), of 4.3×10^{-14} erg cm^{-2} s^{-1}. As we do not have a strong constraint from our Hα image for the broad and double-peaked Hα components contribution, we preferred to use the narrow-line flux of Halpern et al. (1996) to calculate the Hα luminosity of the mini spiral (see Section 5.3).

4. RADIO DATA

4.1. VLA Observations

We obtained archival VLA A- and B-array configuration data at 8 GHz (λ3.6 cm) and B-array configuration data at 5, 8, and 15 GHz (λ6, 3.6, and 2 cm; Experiment code AW230). The observations were carried out on 1993 February 28. 3C 286 was the primary flux density calibrator, while J1740+52 was the phase calibrator for the experiment. The data were processed with the Astronomical Image Processing System (AIPS) software using the standard imaging and self-calibration procedures. The final radio images were made after several iterations of phase and amplitude self-calibrations. Table 1 lists the beam sizes and rms noise in the final radio images.

As is evident from the beam sizes, only the A-array 8 GHz image had sufficient spatial resolution to enable a comparison with our *HST* images. This is illustrated in Figure 4, where the top panel shows the contours of the B-array image and the bottom panel of the A-array image overploted on the Hα structure map. A lot of the discussion ahead focuses on the A-array image.

[10] Using the systemic velocity of 7245 km s^{-1}(de Vaucouleurs et al. 1991) and H_0 = 71 km s^{-1} Mpc^{-1} (Bennett et al. 2003).

Table 1
Summary of VLA Observations

Config	Band	Freq (GHz)	Beam (arcsec^2)	Peak (mJy beam^{-1})	Total (mJy)	rms (μJy beam^{-1})
A	*X*	8	0.23 × 0.19	256	270	27
B	*C*	5	1.45 × 1.11	116	135	26
B	*X*	8	0.75 × 0.61	216	227	75
B	*U*	15	0.42 × 0.33	288	297	25

Note. Column 1: array configuration of the VLA; Column 2: frequency band; Column 3: central frequency in GHz; Column 4: synthesized beam size; Column 5: peak core surface brightness in mJy beam^{-1}; Column 6: total radio flux density in mJy; Column 7: rms noise in image in μJy beam^{-1}.

4.2. Results from the VLA Study

The radio image (Figure 4) shows a one-sided radio jet emerging from the core at a P.A. of ≈90° toward the east and then bending toward the south. The first image of the radio jet was presented by Puschell et al. (1986), although they were then not clear about the radio emission mechanism. Subsequently, Caccianiga et al. (2001) have clearly demonstrated that the parsec-scale radio emission in Arp 102B is from an AGN jet, rather than a starburst, on the basis of its high brightness temperature ($T_b \sim 10^6$–10^8 K). Starbursts typically reveal $T_b < 10^5$ K (Condon et al. 1991). We find that the VLA jet shows two radio knots surrounded by low surface brightness emission. The bending to the south occurs at the first radio knot ∼0.″8 (corresponding to ∼400 pc at the galaxy) from the radio core. Further, the jet seems to flare out after the second radio knot at a distance of ∼1.″3 (∼650 pc). By taking a transverse surface brightness slice and fitting a Gaussian to it (with task SLFIT in AIPS), we found that the jet width increased from ∼0.″25 at a distance of 0.″7, to ∼0.″75 at a distance of 1.″3 away from the core. There is some indication of the beginning of a faint counterjet to the west. However, more sensitive observations are required to confirm this feature. The simplest interpretation for the asymmetry is that the eastern jet is directed partly toward us and is Doppler boosted.

Further evidence for relativistic boosting of the jet comes from milliarcsecond-scale observations with the European VLBI Network (EVN), which detected the radio core and a single additional radio component to the northeast of the nucleus at a P.A. of ≈40° (Caccianiga et al. 2001). Since our A-array image shows the jet emerging at P.A. ≈ 90°, the jet seems to have changed its trajectory considerably. Using the EVN image, we have estimated the jet-to-counterjet surface brightness ratio, R_J, at an approximate projected distance of 0.″02 (9.6 pc) from the radio core. Using the peak surface brightness of the second radio component (see Caccianiga et al. 2001) and assuming the rms noise to be an upper limit to the counterjet surface brightness, we derive an $R_J \geqslant 13$. Assuming the jet structural parameter, $p = 3$ ($p = 2 - \alpha$ for a continuous jet, α being the jet spectral index, defined as $S_\nu \propto \nu^\alpha$; Urry & Padovani 1995), and following the relation, $R_J = ((1+\beta\cos\theta)/(1-\beta\cos\theta))^p$, we obtain $\beta\cos\theta \geqslant 0.4$, where θ is the angle of the radio jet with respect to the line of sight. If we assume that the radio jet is launched perpendicular to the accretion disk, which in turn has its axis inclined at 33° (Chen & Halpern 1989), we obtain a jet velocity of $v \geqslant 0.48c$ at a distance of ∼10 pc from the core. The radio jet in Arp 102B therefore seems to start out relativistically. We note that proper motion studies have indeed detected similar (high) speeds in the parsec-scale jets of some

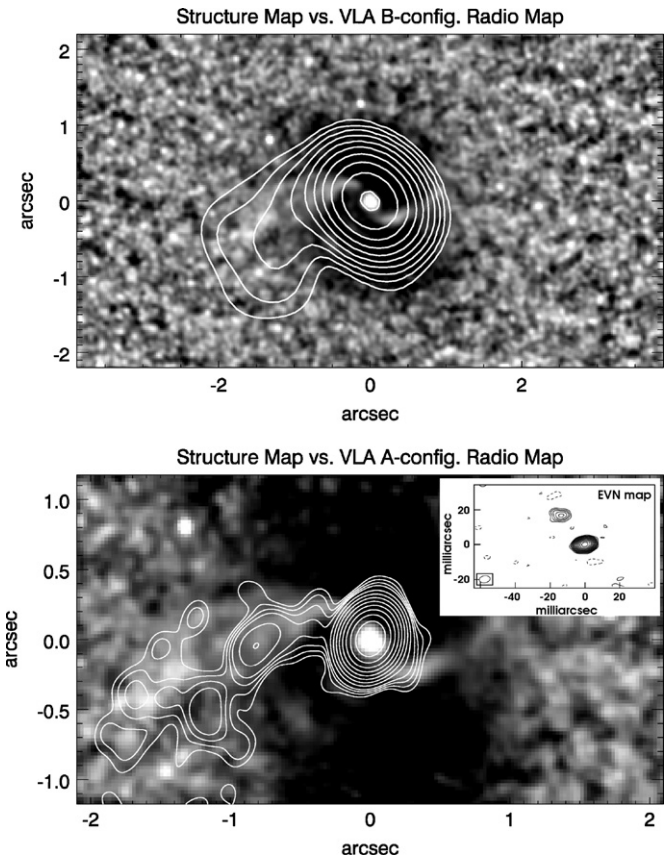

Figure 4. Our *HST*-ACS Hα structure map with overplotted 8 GHz contours of the VLA B-configuration (top panel) and A-configuration (bottom panel) radio images. The radio contours cover a range of (0.08%–90%) of the peak radio flux, while the beam sizes are 0.″75 × 0.″61 at P.A. = 43° in the top panel, and 0.″24 × 0.″19 at P.A. = −18°, in the bottom panel, respectively. The lowest contour indicates a 4σ detection level. The inset image of the inner few tens of milliarcseconds is taken from Caccianiga et al. (2001), and displays the radio core and the radio component at position angle 40°.

Seyferts (e.g., Middelberg et al. 2004). Giroletti et al. (2005) infer a jet speed of ∼0.75c in the S-shaped parsec-scale jet of the LINER galaxy, NGC 4278. The asymmetry in the jet intensity from the famous Seyfert galaxy, NGC 1068, has also been proposed to result from mild relativistic boosting in its jet (e.g., Axon et al. 1998).

We constructed a spectral index image using the B-array 5 GHz and 8 GHz radio images, after first convolving both with a circular beam of size 0.″9 × 0.″9 (Figure 5). We found that while the radio core has an inverted spectral index ($\alpha = 1.15 \pm 0.001$), and the inner jet has a steep spectrum ($\alpha = -1.04 \pm 0.01$, at a distance <1″ from the core), the spectrum steepens considerably in the outer part of the radio structure ($\alpha = -1.95 \pm 0.14$, at a distance of ∼1.″5 from the core). Although the northern edge of the jet shows a clear spectral flattening ($\alpha = -0.46 \pm 0.15$) at a distance of ∼1.″5 from the radio core (see top panel of Figure 4), which could be indicative of a jet shock, the spatial resolution in the spectral index image is not sufficient to make a one-to-one comparison with features in the *HST* image. The 15 GHz B-array image could resolve only the inner jet structure (<1″ from the core) and the 8–15 GHz spectral index image did not reveal any more detail than the 5–8 GHz spectral index image. The overall radio morphology and the 5–8 GHz spectral index image could however be considered as being consistent with the picture of a radio jet impacting emission-line clouds in the nuclear interstellar medium (ISM).

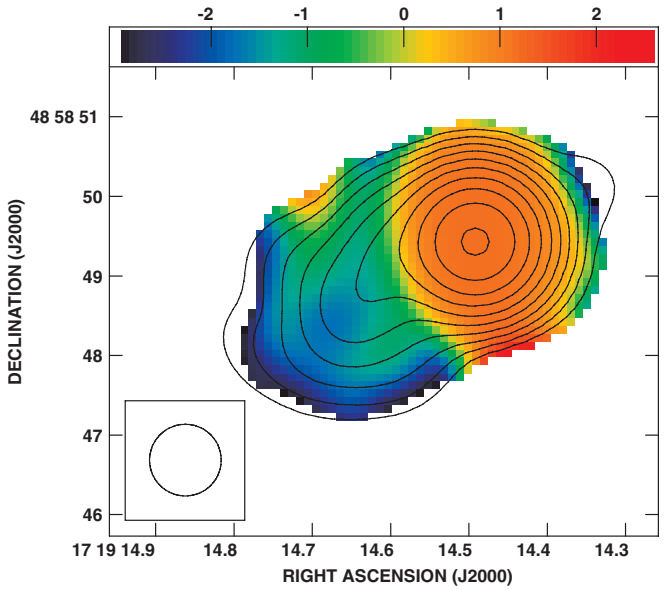

Figure 5. 5–8 GHz spectral index map of Arp 102B made with a 0.″9 circular beam. The 5 GHz total intensity contours are superimposed.
(A color version of this figure is available in the online journal.)

Under the assumption of "equipartition" of energy between relativistic particles and the magnetic field (Burbidge 1959), we estimated the minimum magnetic field strength and other parameters for a cylindrical jet geometry. The total radio luminosity was estimated assuming that the radio spectrum extends from 10 MHz to 10 GHz with a spectral index of $\alpha = -1$. Furthermore, it was assumed that the relativistic protons and electrons have equal energies, and the radio emitting plasma has a volume filling factor of unity. From the 8 GHz image, we estimate the integrated jet flux density to be ∼270 mJy and the size of the radio jet to be 2.″5 × 1.″3. Following the relations in O'Dea & Owen (1987), we obtain a total radio luminosity of $L_{\rm rad} = 1.9 \times 10^{41}$ erg s^{-1}, a minimum magnetic field of $B_{\rm min} \sim 0.1$ mG, minimum energy of $E_{\rm min} = 2.9 \times 10^{55}$ ergs, and a minimum pressure of $P_{\rm min} = 1.2 \times 10^{-9}$ dynes cm^{-2}.

The electron lifetime due to synchrotron radiative losses can be estimated using the relation $t_{\rm syn} \simeq 33.4 B_{10}^{-3/2} \nu_c^{-1/2}$ Myr, where B_{10} is the magnetic field ("minimum" B field here) in units of 10 μG, and ν_c is the critical frequency in GHz (e.g., Pacholczyk 1970). This turns out to be $\sim 3 \times 10^5$ yr for a critical frequency of 8 GHz. Further assuming that the efficiency (ϵ) with which the total jet energy is tapped to produce radio luminosity is 1% (e.g., O'Dea 1985), the jet would have a kinetic luminosity ($L_{\rm rad}/\epsilon$) of $\sim 1.9 \times 10^{43}$ erg s^{-1}. Following the relation derived by Bîrzan et al. (2004) for radio-filled cavities, we also derive a jet kinetic luminosity of $\sim 1.1 \times 10^{43}$ erg s^{-1}.

5. DISCUSSION

Our observations have revealed an apparent two-arm grand-design nuclear spiral structure in Arp 102B, extending from ≈50 pc up to more than 500 pc from the nucleus. We now discuss two possibilities for the origin of these spiral arms, namely that they are formed either through some dynamical process, or by jet–cloud interaction.

5.1. A Dynamical Formation Scenario

The spiral structure that we find in our high-resolution *HST*-ACS image could be described as a grand-design nuclear spiral. Similar grand-design nuclear spirals have been previously found around the nucleus of many Seyfert galaxies (Martini & Pogge 1999). Maciejewski et al. (2002) and Maciejewski (2004b) argue that such grand-design spirals are shocks in the gas, leading to dissipation and inflow.

A strong correlation between the presence of an AGN and the presence of dusty nuclear spirals was found by Simões Lopes et al. (2007) in *HST* optical images of a sample of early-type hosts. Pogge & Martini (2002, p. 624) also find nuclear spirals in almost all Seyfert galaxies of their sample. They also argue that there is "a clear physical connection between the nuclear dust spirals on hundreds of parsec scales and large-scale bars and spiral arms in the host galaxies proper." In disk galaxies, theoretical works show how the presence of a non-axisymmetric potential is efficient in disturbing the circular orbits of gas and stars, and to cause a loss of angular momentum due to torques and shocks (e.g., Schwarz 1984). This process results in infall of matter from the outer parts toward the center of the gravitational potential (e.g., Combes & Gerin 1985; Knapen et al. 1995; Jogee et al. 2002; Fathi et al. 2007). It is thus possible that large-scale non-axisymmetric potentials lead to the formation of an inner structure, which in turn can lead the gas further inward (e.g., Maciejewski & Sparke 2000; Emsellem et al. 2001; Heller et al. 2001; Shlosman 2001, 2005; Maciejewski 2004a, 2004b). In the case of elliptical galaxies, there is indication that—in at least half of them—the gas observed in the nuclear region comes from outside of the system (Sarzi et al. 2006). Thus, in elliptical galaxies with no sign of a gaseous disk, gas gets to the centers usually because a ballistic cloud undergoes dynamical friction and spirals in, and then the cloud's angular momentum may spread it into a disk in the central kpc.

Nuclear spirals and filaments have been detected via the contrast produced by the associated dust in broadband images of essentially all nearby active galaxies (e.g., Malkan et al. 1998; Simões Lopes et al. 2007). For a few of them, mass inflows in ionized and molecular gas associated to nuclear spirals have been recently mapped down to a few parsecs or tens of parsecs of the AGN. Examples are the gas kinematic studies around the active nuclei of the galaxies NGC 7469 (Davies et al. 2004), NGC 1097 (Fathi et al. 2005, 2006; Davies et al. 2009; van de Ven & Fathi 2010), NGC 6951 (Storchi-Bergmann et al. 2007), NGC 4051 (Riffel et al. 2008), NGC 7582 (Riffel et al. 2009), NGC 4151 (Storchi-Bergmann et al. 2010), NGC 1068 (Müller Sánchez et al. 2009), and M81 (Schnorr Müller et al. 2011).

Similarly, the nuclear spiral in Arp 102B may also trace a gas inflow. A possibility is that the current nuclear activity in Arp 102B is being fueled by gas acquired from the companion galaxy Arp 102A, as Arp 102B lies at the end of the tidal arms of Arp 102A. This interaction may have fed gas into the galaxy and this gas may then have found its way to nuclear scales—via the mechanisms discussed above—to feed the AGN. We can calculate the amount of gas available for accretion using the Hα flux from Halpern et al. (1996), as discussed in Section 3, of 4.3 $\times 10^{-14}$ erg cm^{-2} s^{-1} and an adopted distance to Arp 102B of 102 Mpc, to obtain the Hα luminosity of $L_{\rm H\alpha} = 5.4 \times 10^{40}$ erg s^{-1}. The ionized gas mass M can be obtained (Osterbrock & Ferland 2006) from

$$M = m_p \frac{L_{\rm H\alpha}}{3.56 \times 10^{-25} N_e}, \quad (2)$$

where m_p is the mass of the proton in grams, and N_e is the electronic density in cm^{-3}. For a gas density of 100 cm^{-3} (estimated from the [S II]λ6731/λ6717 line ratio in Halpern

et al. 1996), this gives a total ionized gas mass for the spiral of $M = 1.3 \times 10^6$ solar masses. Considering the uncertainties in the Hα flux as well as in the gas density, the resulting uncertainty in the calculated gas mass is a factor of $\approx$2.

5.2. A Jet–Cloud Interaction

The highly curved radio jet and its good overall spatial coincidence with the emission-line gas forming the eastern arm of the spiral suggests a scenario in which an initially relativistic, possibly precessing, radio jet shocks and ionizes the surrounding gas. This is also suggested by the orientation of the milliarcsecond VLBI structure, at P.A. = 40°, which coincides with the orientation of the inner part of the east spiral arm. In this case, the spiral arms could be formed from shocks which arise when the radio jet makes its way through the ISM (e.g., Veilleux et al. 1993; Veilleux et al. 2005). Both jet-like emission-line structures and kinematically disturbed ionized gas associated with the radio jets have been found previously in a number of nearby Seyfert galaxies, e.g., Mrk 6 and NGC 1068 (Gallimore et al. 1996; Capetti et al. 1997; Axon et al. 1998).

It could be argued that the apparent bending of the jet in this "radio-quiet" AGN, from a P.A. $\approx$ 40° on milliarcsecond scales to $\approx$110° on arcsecond scales (Figure 4), could be due to the "deflection" of the radio jet by an ISM cloud, as observed in other AGNs such as NGC 1068 (Gallimore et al. 1996). This is supported in the case of NGC 1068 by a sharp change in the jet direction of $\approx$20°. However, in the Arp 102B jet there is no sharp bend, and the "smooth" continuous change of direction from pc to kpc scales can rather be attributed either to a viewing angle effect or precession. In the former case, the jet would have to be relativistic and at a relatively low (<45°) inclination, which—as we have already argued—is consistent with a relativistic boosting explanation for its one-sidedness. Alternatively, the change in direction could result from jet precession, an effect that has been invoked to explain similar features in several Seyfert galaxies, e.g., NGC 3079 (Baan & Irwin 1995), Mrk 6 (Kharb et al. 2006), NGC 6764 (Kharb et al. 2010a), and radio-loud AGNs (Conway & Murphy 1993; Kharb et al. 2010b), and may be a consequence either of instabilities in the accretion disk or the presence of a binary black hole.

Finally, it could be also conjectured that the apparent alignment between the arcsec-scale radio jet and the eastern arm is due to a chance projection of a foreshortened jet. This is very unlikely because there is a very good correspondence between the east arm in the radio image and the one in the Hα image. However, our current data do not allow a more detailed discussion.

5.3. Ionization Mechanism

In Section 4.2, we estimated a kinetic luminosity for the radio jet of $(L_{\rm rad}/\epsilon)$ of $\sim 1.9 \times 10^{43}$ erg s^{-1}, which we can compare to the Hα luminosity of the extended emission of 5.4×10^{40} erg s^{-1}. This is much smaller than the kinetic luminosity of the jet, which is therefore energetically capable of ionizing the emission-line gas. The jet kinematic energy would be transferred to the gas via shocks. In a fast shock (Sutherland et al. 1993; Allen et al. 2008), optical emission lines are expected to arise both in the collisionally ionized gas forming the downstream cooling flow, and via photoionization of upstream gas by X-rays emitted by hot gas immediately behind the shock. In either case, shock velocities $\geqslant$100 km s^{-1} are required, implying comparable line widths for the emission arising in the shocked gas, while the widths of lines produced by the photoionized precursor would reflect the local velocity field of the undisturbed gas. For comparison, the narrow-line FWHM, as measured by Halpern et al. (1996), are $\sim$400–600 km s^{-1}.

Alternatively, the emission-line gas in the arms could be photoionized by the UV–X-ray continuum of the AGN itself. The optical–UV spectrum of Arp 102B falls steeply into the UV ($f_\nu \propto \nu^{-2.1}$; Halpern et al. 1996) and thus contributes little flux above the Lyman limit. On the other hand, the 0.5–10 keV X-ray spectrum is well described by an absorbed power law of photon index $\Gamma \approx 1.6$ (Eracleous et al. 2003), as is typical of Seyfert 1 galaxies. If this extends to the Lyman limit, it would provide sufficient ionizing photons to account for the Hα emission in the arms. Assuming all photons with energies $13.6\,{\rm eV} \leqslant h\nu \leqslant 54.4$ eV are absorbed by hydrogen, the total Hα flux is given by

$$F_{\rm H\alpha} = \frac{\alpha_{\rm H\alpha}^{\rm eff}}{\alpha_{\rm B}} \left(\frac{\nu_{\rm H\alpha}}{\nu_{1\,\rm keV}}\right) F_{1\,\rm keV} \int_{\nu_{\rm H\,I}}^{\nu_{\rm He\,II}} \left(\frac{\nu}{\nu_{1\,\rm keV}}\right)^{-(\alpha+1)} d\nu, \quad (3)$$

where $\alpha_{\rm H\alpha}^{\rm eff}$ and $\alpha_{\rm B}$ are, respectively, the effective recombination coefficient for Hα and the total case B recombination coefficient (Osterbrock & Ferland 2006) and the various frequencies are identified by their subscripts. Taking the 1 keV flux given by Eracleous et al., $F_{1\,\rm keV} \approx 1.7\,\mu$Jy, and $\alpha = \Gamma - 1$, we find $F_{\rm H\alpha} \sim 4 \times 10^{-14}$ erg s^{-1} cm^{-2}, consistent with the observed Hα flux.

A detailed discussion of the line intensity ratios is beyond the scope of the present paper. We merely note that LINER spectra have been interpreted both in terms of shocks (Dopita & Sutherland 1995) and photoionization by a dilute, hard radiation field (e.g., Terashima et al. 2000; Ferland & Netzer 1983). Stauffer et al. (1983) argued that shocks are most likely responsible for ionizing the narrow-line region in Arp 102B, citing among other things, the high electron temperature ($T >$ 30,000 K) implied by the strength of the [O III]λ4363 line, relative to [O III]λ5007. However, this line is relatively weak and Halpern et al. note that their measured flux for this line is highly uncertain. Two-dimensional spectroscopy of the "arms" would help to distinguish between central source photoionization and shocks associated with the radio jet.

6. SUMMARY

We report the discovery of a two-armed gaseous spiral structure in the central kiloparsec ($\approx 2''$) of the E0 LINER/Seyfert 1 galaxy Arp 102B in an *HST*-ACS Hα emission-line gas image and adjacent continuum.

Our morphological analysis has enabled us to trace the spiral arms from $0\farcs1$ ($\approx$50 pc) to more than $1''$ ($\approx$500 pc) from the nucleus to the east and west of the nucleus. Previous studies by our group have shown that spiral arms in the nuclear region of active galaxies can be channels to feed the SMBH, as in a few cases studied so far inflows have been found along such arms. In the case of Arp 102B, a possible trigger for sending gas inward could be its companion galaxy Arp 102A. We calculate the mass of ionized gas of the spiral to be $M \approx 10^6$ solar masses. We speculate that the recent accretion of gas to the AGN in Arp 102B is related to its double-peaked emission-line profiles, presumably originating in the outer parts of a recently replenished accretion disk.

Nevertheless, archival VLA observations of Arp 102B reveal a one-sided radio jet structure which is well aligned with the east spiral arm, which suggests that the arms originate in a jet–cloud

interaction. A milliarcsecond radio structure also aligns with the orientation of the inner part of the eastern spiral arm. Thus, although the origin of the gas in the nuclear spiral may have been a recent accretion event, which probably triggered the nuclear activity producing the observed radio jet, the present observations suggest the alternative interpretation that the Hα spiral arms are a result of the interaction between the jet and the remaining circumnuclear gas.

The kinetic energy delivered by the jet is sufficient to ionize the Hα emitting gas. However, it could also be photoionized by AGN X-ray continuum; the morphological relationship could simply be due to an increased emission measure where shocks have compressed the surrounding gas. The absence of a radio counterjet coincident with the western arm seen in the Hα image can be explained if the jet is relativistic. This is further supported by the milliarcsecond structure which shows only one extranuclear component at P.A. $\approx 40^{\circ}$. An estimate for the relativistic particle speed in the inner part of the jet is $0.45c$.

Based on observations with the NASA/ESA *Hubble Space Telescope* obtained at the Space Telescope Science Institute, which is operated by the Association of Universities for Research in Astronomy, Inc., under NASA contract NAS5-26555. The National Radio Astronomy Observatory is a facility of the National Science Foundation operated under cooperative agreement by Associated Universities, Inc. We thank an anonymous referee for a careful reading of the manuscript and useful suggestions which helped to improve the paper. T.S.-B. acknowledges support from the Brazilian institution CNPq. K.F. acknowledges financial support from NASA through grant number *HST*-GO 09782.01, from the Royal Swedish Academy of Sciences, and from the Swedish Research Council.

REFERENCES

Allen, M. G., Groves, B. A., Dopita, M. A., Sutherland, R. S., & Kewley, L. J. 2008, ApJS, 178, 20
Axon, D. J., Marconi, A., Capetti, A., Macchetto, F. D., Schreier, E., & Robinson, A. 1998, ApJ, 496, L75
Baan, W. A., & Irwin, J. A. 1995, ApJ, 446, 602
Barth, A. J., Ho, L. C., Filippenko, A. V., Rix, H.-W., & Sargent, W. L. W. 2001, ApJ, 546, 205
Bennett, C. L., et al. 2003, ApJS, 148, 1
Bîrzan, L., Rafferty, D. A., McNamara, B. R., Wise, M. W., & Nulsen, P. E. J. 2004, ApJ, 607, 800
Bower, G. A., Wilson, A. S., Heckman, T. M., & Richstone, D. O. 1996, AJ, 111, 1091
Burbidge, G. R. 1959, ApJ, 129, 849
Caccianiga, A., Marchã, M. J. M., Thean, A., & Dennett-Thorpe, J. 2001, MNRAS, 328, 867
Capetti, A., Axon, D. J., & Macchetto, F. D. 1997, ApJ, 487, 560
Chen, K., & Halpern, J. P. 1989, ApJ, 344, 115
Chen, K., Halpern, J. P., & Filippenko, A. V. 1989, ApJ, 339, 742
Combes, F., & Gerin, M. 1985, A&A, 150, 327
Condon, J. J., Huang, Z.-P., Yin, Q. F., & Thuan, T. X. 1991, ApJ, 378, 65
Conway, J. E., & Murphy, D. W. 1993, ApJ, 411, 89
Davies, R. I., Maciejewski, W., Hicks, E. K. S., Tacconi, L. J., Genzel, R., & Engel, H. 2009, ApJ, 702, 114
Davies, R. I., Tacconi, L. J., & Genzel, R. 2004, ApJ, 602, 148
de Vaucouleurs, G., de Vaucouleurs, A., Corwin, H. H., Buta, R. J., Paturel, G., & Fouque, P. 1991, Third Reference Catalogue of Bright Galaxies (New York: Springer)
Dopita, M. A., & Sutherland, R. S. 1995, ApJ, 455, 468
Elmegreen, B. G., et al. 1998, ApJ, 503, L119
Emsellem, E., Goudfrooij, P., & Ferruit, P. 2003, MNRAS, 345, 1297
Emsellem, E., Greusard, D., Combes, F., Friedli, D., Leon, S., Pécontal, E., & Wozniak, H. 2001, A&A, 368, 52
Englmaier, P., & Shlosman, I. 2000, ApJ, 528, 677
Eracleous, M., & Halpern, J. P. 1994, ApJS, 90, 1
Eracleous, M., Halpern, J. P., & Charlton, J. C. 2003, ApJ, 582, 633
Fathi, K. 2004, PhD thesis, University of Groningen
Fathi, K., Beckman, J. E., Zurita, A., Relaño, M., Knapen, J. H., Daigle, O., Hernandez, O., & Carignan, C. 2007, A&A, 466, 905
Fathi, K., Storchi-Bergmann, T., Riffel, R. A., Winge, C., Axon, D. J., Robinson, A., Capetti, A., & Marconi, A. 2006, ApJ, 641, L25
Fathi, K., van de Ven, G., Peletier, R. F., Emsellem, E., Falcón-Barroso, J., Cappellari, M., & de Zeeuw, P. T. 2005, MNRAS, 364, 773
Ferland, G. J., & Netzer, H. 1983, ApJ, 264, 105
Flohic, H. M. L. G., & Eracleous, M. 2008, ApJ, 686, 138
Gallimore, J. F., Baum, S. A., & O'Dea, C. P. 1996, ApJ, 464, 198
Gezari, S., Halpern, J., & Eracleous, M. 2007, ApJS, 169, 167
Giroletti, M., Taylor, G. B., & Giovannini, G. 2005, ApJ, 622, 178
Halpern, J. P., Eracleous, M., Filippenko, A., & Chen, K. 1996, ApJ, 464, 704
Heller, C. H., Shlosman, I., & Englmaier, P. 2001, ApJ, 553, 661
Ho, L. C., Rudnick, G., Rix, H.-W., Shields, J. C., McIntosh, D. H., Filippenko, A. V., Sargent, W. L. W., & Eracleous, M. 2000, ApJ, 541, 120
Jogee, S., Scoville, N., & Kenney, J. D. P. 2005, ApJ, 630, 837
Jogee, S., Shlosman, I., Laine, S., Englmaier, P., Knapen, J. H., Scoville, N., & Wilson, C. D. 2002, ApJ, 575, 156
Kharb, P., Hota, A., Croston, J. H., Hardcastle, M. J., O'Dea, C. P., Kraft, R. P., Axon, D. J., & Robinson, A. 2010a, ApJ, 723, 580
Kharb, P., Lister, M. L., & Cooper, N. J. 2010b, ApJ, 710, 764
Kharb, P., O'Dea, C. P., Baum, S. A., Colbert, E. J. M., & Xu, C. 2006, ApJ, 652, 177
Knapen, J. H., Beckman, J. E., Heller, C. H., Shlosman, I., & de Jong, R. S. 1995, ApJ, 454, 623
Krist, J., & Hook, R. 1999, The Tiny Tim User's Guide, Version 5.0 (Baltimore, MD: STScI)
Lewis, K., Eracleous, M., & Storchi-Bergmann, T. 2010, ApJS, 187, 416
Lucy, L. B. 1974, AJ, 79, 745
Maciejewski, W. 2004a, MNRAS, 354, 883
Maciejewski, W. 2004b, MNRAS, 354, 892
Maciejewski, W., & Sparke, L. S. 2000, MNRAS, 313, 745
Maciejewski, W., Teuben, P. J., Sparke, L. S., & Stone, J. M. 2002, MNRAS, 329, 502
Malkan, M., Gorjian, V., & Tam, R. 1998, ApJS, 117, 25
Martini, P., & Pogge, R. W. 1999, AJ, 118, 2646
Martini, P., Regan, M. W., Mulchaey, J. S., & Pogge, R. W. 2003, ApJS, 146, 353
Middelberg, E., et al. 2004, A&A, 417, 925
Montenegro, L. E., Yuan, C., & Elmegreen, B. G. 1999, ApJ, 520, 592
Müller Sánchez, F., Davies, R. I., Genzel, R., Tacconi, L. J., Eisenhower, F., Hicks, E. K. S., Friederich, S., & Sterneberg, A. 2009, ApJ, 691, 749
Newman, J. A., Eracleous, M., Filippenko, A. V., & Halpern, J. P. 1997, ApJ, 485, 570
O'Dea, C. P. 1985, ApJ, 295, 80
O'Dea, C. P., & Owen, F. N. 1987, ApJ, 316, 95
Osterbrock, D. E., & Ferland, G. 2006, Astrophysics of Gaseous Nebulae and AGN (2nd ed.; Mill Valley, CA: University Science Books)
Pacholczyk, A. G. (ed.) 1970, Radio Astrophysics: Nonthermal Processes in Galactic and Extragalactic Sources (San Francisco, CA: Freeman)
Pavlovsky, C., et al. 2005, ACS Data Handbook, Version 4.0 (Baltimore, MD: STScI)
Pogge, R. W., & Martini, P. 2002, ApJ, 569, 624
Puschell, J. J., Moore, R., Cohen, R. D., Owen, F. N., & Phillips, A. C. 1986, AJ, 91, 751
Richardson, W. H. 1972, J. Opt. Soc. Am., 62, 55
Riffel, R., Storchi-Bergmann, T., Dors, O. L., & Winge, C. 2009, MNRAS, 393, 783
Riffel, R., Storchi-Bergmann, T., Winge, C., McGregor, P., Beck, T., & Schmitt, H. R. 2008, MNRAS, 385, 1129
Saijo, M., Baumgarte, T. W., & Shapiro, S. L. 2003, ApJ, 595, 352
Sarzi, M., et al. 2006, MNRAS, 366, 1151
Schnorr Müller, A., Storchi-Bergmann, T., Riffel, R. A, Ferrari, F., Steiner, J. E., Axon, D. J., & Robinson, A. 2011, MNRAS, 413, 149
Schwarz, M. P. 1984, MNRAS, 209, 93
Shields, J. C., Rix, H.-W., McIntosh, D. H., Ho, L. C., Rudnick, G., Filippenko, A. V., Sargent, W. L. W., & Sarzi, M. 2000, ApJ, 534, L27
Shlosman, I. 2001, in ASP Conf. Ser. 249, The Central Kiloparsec of Starbursts and AGN: The La Palma Connection, ed. J. H. Knapen, J. E. Beckman, I. Shlosman, & T. J. Mahoney (San Francisco, CA: ASP), 55

Shlosman, I. 2005, in AIP Conf. Proc. 783, The Evolution of Starbursts: The 331st Wilhelm and Else Heraeus Seminar, ed. S. Hüttmeister, E. Manthey, & D. Bomans (Melville, NY: AIP), 223
Simões Lopes, R. D., Storchi-Bergmann, T., Saraiva, M. F., & Martini, P. 2007, ApJ, 655, 718
Snyder, D. L., Hammoud, A. M., & White, R. L. 1993, J. Opt. Soc. Am. A, 10, 1014
Stauffer, J., Schild, R., & Keel, W. 1983, ApJ, 270, 465
Storchi-Bergmann, T., Baldwin, J. A., & Wilson, A. S. 1993, ApJ, 410, L11
Storchi-Bergmann, T., Dors, O. L., Jr., Riffel, R. A., Fathi, K., Axon, D. J., Robinson, A., Marconi, A., & Östlin, G. 2007, ApJ, 670, 959
Storchi-Bergmann, T., Lopes, R. D. S., McGregor, P. J., Riffel, R. A., Beck, T., & Martini, P. 2010, MNRAS, 402, 819
Storchi-Bergmann, T., Rodriguez-Ardila, A., Schmitt, H. R., Wilson, A. S., & Baldwin, J. A. 1996, ApJ, 472, 83
Storchi-Bergmann, T., et al. 2003, ApJ, 598, 956
Sutherland, R. S., Bicknell, G. V., & Dopita, M. A. 1993, ApJ, 414, 510
Terashima, Y., Ho, L. C., & Ptak, A. F. 2000, ApJ, 539, 161
Urry, C. M., & Padovani, P. 1995, PASP, 107, 803
van de Ven, G., & Fathi, K. 2010, ApJ, 723, 767
Veilleux, S., Cecil, G., & Bland-Hawthorn, J. 2005, ARA&A, 43, 769
Veilleux, S., Tully, R. B., & Bland-Hawthorn, J. 1993, AJ, 105, 1318
Yuan, C., & Yen, D. C. C. 2004, in Astrophys. Space Sci. Lib. Vol. 319, Penetrating Bars Through Masks of Cosmic Dust, ed. D. Block et al. (Dordrecht: Kluwer), 703